Inorganic Chemistry
Article

Inorg. Chem. **2010**, *49*, 10001–10006 **10001**
DOI: 10.1021/ic101294s

A Series of (6,6)-Connected Porous Lanthanide−Organic Framework Enantiomers with High Thermostability and Exposed Metal Sites: Scalable Syntheses, Structures, and Sorption Properties

Hai-Long Jiang,[†] Nobuko Tsumori,[†,‡] and Qiang Xu*[,†]

[†]*National Institute of Advanced Industrial Science and Technology (AIST), Ikeda, Osaka 563-8577, Japan, and*
[‡]*Toyama National College of Technology, 13 Hongo-machi, Toyama 939-8630, Japan*

Received June 29, 2010

A series of microporous lanthanide−organic framework enantiomers, $Ln(BTC)(H_2O)\cdot(DMF)_{1.1}$ (Ln = Y **1a**, **1b**; Tb **2a**, **2b**; Dy **3a**, **3b**; Er **4a**, **4b**; Yb **5a**, **5b**, BTC = 1,3,5-benzenetricarboxylate; DMF = *N*,*N*-dimethylformamide) with unprecedented (6,6)-connected topology have been prepared and characterized. All these compounds exhibit very high thermal stability of over 450 °C. The pore characteristics and gas sorption properties of these compounds were investigated at cryogenic temperatures by experimentally measuring nitrogen, argon, and hydrogen adsorption/desorption isotherms. The studies show that all these compounds are highly porous with surface areas of 1080 (**1**), 786 (**2**), 757 (**3**), 676 (**4**), and 774 m^2/g (**5**). The amounts of the hydrogen uptakes, 1.79 (**1**), 1.45 (**2**), 1.40 (**3**), 1.51 (**4**), and 1.41 wt % (**5**) at 77 K (1 atm), show their promising H_2 storage performances. These porous materials with considerable surface areas, high voids of 44.5% (**1**), 44.8% (**2**), 47.7% (**3**), 44.2% (**4**), and 45.7% (**5**), free windows of 6−7 Å, available exposed metal sites and very high thermal stability can be easily prepared on a large scale, which make them excellent candidates in many functional applications, such as, gas storage, catalysis, and so on.

Introduction

Porous metal−organic frameworks (MOFs) are currently of great interests not only because of their intriguing variety of architectures but also because of their tremendous potential applications in chemical sensing, catalysis, and gas storage and separations, etc.[1−3] By the perception of the rapid developments on MOF field, actually, a great deal of research work focuses on the syntheses and applications of the nanopores. The designable and continuously tunable pore systems in MOF materials ranging from the ultramicroporous to mesoporous have been reported, which make MOFs bridge the gap between mesoporous silica with large pores and zeolites with limited pores.[1e] The porosity in MOFs plays crucial roles in gas storage and separation, transporting organic substrates and products in catalysis, etc.[1b,4] Meanwhile, the application of pores closely relates to the stability of MOFs, which is usually low and a disadvantage in MOFs in contrast to traditional porous materials (zeolites, mesoporous silica, etc.).[4b,f] Therefore, it is exigent but challenging to obtain MOFs with both high porosity and stability. On the other hand, the design and construction of chiral MOFs are receiving growing attention because of their intriguing potential applications, especially for enantioselective catalysis and separation.[4a−c] So far, in the limited reports on chiral MOFs, mostly of which were synthesized by choosing chiral species (chiral organic linkers or chiral metal complexes) as structure directing agents.[4a,b] While without any chiral auxiliary, to obtain a chiral compound by using achiral ligand

*To whom correspondence should be addressed. E-mail: q.xu@aist.go.jp.

(1) (a) Moulton, B.; Zaworotko, M. J. *Chem. Rev.* **2001**, *101*, 1629. (b) Eddaoudi, M.; Kim, J.; Rosi, N.; Vodak, D.; Wachter, J.; O'Keeffe, M.; Yaghi, O. M. *Science* **2002**, *295*, 469. (c) Férey, G.; Mellot-Draznieks, C.; Serre, C.; Millange, F.; Dutour, J.; Surblé, S.; Margiolaki, I. *Science* **2005**, *309*, 2040. (d) Horike, S.; Shimomura, S.; Kitagawa, S. *Nat. Chem.* **2009**, *1*, 695. (e) Farrusseng, D.; Aguado, S.; Pinel, C. *Angew. Chem., Int. Ed.* **2009**, *48*, 7502.
(2) (a) Pan, L.; Parker, B.; Huang, X. Y.; Olson, D. H.; Lee, J. Y.; Li., J. *J. Am. Chem. Soc.* **2006**, *128*, 4180. (b) Du, M.; Jiang, X. J.; Zhao, X. J. *Chem. Commun.* **2005**, 5521. (c) Huang, Y. G.; Wu, B. L.; Yuan, D. Q.; Xu, Y. Q.; Jiang, F. L.; Hong, M. C. *Inorg. Chem.* **2007**, *46*, 1171.
(3) (a) Sun, D. F.; Ma, S. Q.; Ke, Y. X.; Collins, D. J.; Zhou, H. C. *J. Am. Chem. Soc.* **2006**, *128*, 3896. (b) Chen, B.; Yang, Y.; Zapata, F.; Lin, G.; Qian, G.; Lobkovsky, E. B. *Adv. Mater.* **2007**, *19*, 1693. (c) Bradshaw, D.; Warren, J. E.; Rosseinsky, M. J. *Science* **2007**, *315*, 977. (d) Fang, Q.-R.; Zhu, G.-S.; Jin, Z.; Ji, Y.-Y.; Ye, J.-W.; Xue, M.; Yang, H.; Wang, Y.; Qiu, S.-L. *Angew. Chem., Int. Ed.* **2007**, *46*, 6638. (e) Jiang, H. L.; Liu, B.; Akita, T.; Haruta, M.; Sakurai, H.; Xu, Q. *J. Am. Chem. Soc.* **2009**, *131*, 11302.
(4) (a) Seo, J. S.; Whang, D.; Lee, H.; Jun, S. I.; Oh, J.; Jeon, Y. J.; Kim, K. *Nature* **2000**, *404*, 982. (b) Wu, C.-D.; Hu, A.; Zhang, L.; Lin, W. *J. Am. Chem. Soc.* **2005**, *127*, 8940. (c) Ma, L. Q.; Abney, C.; Lin, W. B. *Chem. Soc. Rev.* **2009**, *38*, 1248. (d) Pan, L.; Olson, D. H.; Ciemnolonski, L. R.; Heddy, R.; Li, J. *Angew. Chem., Int. Ed.* **2006**, *45*, 616. (e) Lin, X.; Telepeni, I.; Blake, A. J.; Dailly, A.; Brown, C. M.; Simmons, J. M.; Zoppi, M.; Walker, G. S.; Thomas, K. M.; Mays, T. J.; Hubberstey, P.; Champness, N. R.; Schröder, M. *J. Am. Chem. Soc.* **2009**, *131*, 2159. (f) Cheon, Y. E.; Suh, M. P. *Angew. Chem., Int. Ed.* **2009**, *48*, 2899. (g) Jiang, H.-L.; Tastu, Y.; Lu, Z.-H.; Xu, Q. *J. Am. Chem. Soc.* **2010**, *132*, 5586.

Published on Web 10/06/2010

under spontaneous resolution is possible but harder, because of the great difficulty to achieve interlinking of the chiral molecular units into a homochiral structure with high dimensionality and to induce spontaneous resolution.[5] So far, there have been numerous achiral porous metal−organic frameworks with high surface areas obtained based on various synthetic strategies, while chiral porous MOFs are still rarely reported.[6b,7] Although porosity, stability and chirality play coequally important roles in chemistry, catalysis and biology, it is still challenging to design a crystalline material containing all these properties.[6] In this work, we present the first series of enantiomerically pure chiral 3D lanthanide-based organic frameworks, $Ln(BTC)(H_2O)\cdot(DMF)_{1.1}$ (Ln = Y **1a**, **1b**; Tb **2a**, **2b**; Dy **3a**, **3b**; Er **4a**, **4b**; Yb **5a**, **5b**, BTC = 1,3,5-benzenetricarboxylate; DMF = *N*,*N*-dimethylformamide), which are constructed from achiral ligands under spontaneous resolution without any chiral auxiliary. Furthermore, all these MOFs are highly thermostable and permanently porous with high surface areas and they show high potentials for H_2 storage. It should be noted here that although four compounds of **1a**, **2a**, **3a**, and **5a** with $P4_122$ space group were reported recently by different research groups, all of them failed to obtain their enantiomers.[8] We have successfully obtained all the spontaneous-resolution conglomerations in a one-pot reaction with large-scale, high purity and yields. Considering the importance of **1a**, **2a**, **3a**, and **5a** and the system of study, they are listed, characterized and discussed together.

Experimental Section

Materials and General Methods. All the solvents and reagents for syntheses were commercially available and used as received. IR spectra were recorded on an attenuated total reflectance (ATR) FT-IR spectrometer (SensIR Technologies). Elemental analyses were performed on a Perkin-Elmer 2400 Series II analyzer. Thermogravimetric analyses (TGA) were carried out on a Shimadzu DTG-50 thermal analyzer from room temperature to 600 °C at a ramp rate of 5 °C/min in air. Powder X-ray diffraction (PXRD) studies were carried out with an X-ray diffractometer of Rigaku, Rint 2000. The nitrogen, argon and hydrogen adsorption/desorption isotherms were measured using automatic volumetric adsorption equipments (BELSORP, BEL Japan, Inc., for N_2 and Ar and Mircomeritics, ASAP2010 for H_2). All the samples were subjected to solvent exchange (by soaking in methanol for over 1 day and then changing to dichloromethane for over 1 day) and evacuation at 350 °C overnight prior to the adsorption/desorption measurement.

Preparations of Compounds 1−5. Preparations of Y(BTC)-$(H_2O)\cdot(DMF)_{1.1}$ (1a and 1b). A mixture of $Y(NO_3)_3\cdot 6H_2O$ (0.191 g, 0.5 mmol), BTC (0.053 g, 0.25 mmol), DMF (4 mL), and H_2O (4 mL) was sealed in a 24 mL of Teflon-lined reactor. The pure colorless needle crystals with yield of ∼58% containing **1a** and **1b** were obtained after 24 h of heating at 105 °C. Moreover, the gram-scale pure crystals of **1a** and **1b** can be easily obtained by scaling up the reactant quantities in a 132 mL of Teflon reactor. Calcd for $Y(C_9H_3O_6)(H_2O)(C_3H_6ON)_{1.1}$: C, 37.56; H, 2.98; N, 3.92. Found: C, 37.72; H, 3.02; N, 3.90. IR (cm^{-1}): 1611 m, 1572 w, 1536 w, 1433 m, 1372 s, 1103 w, 939 w, 772 s, 714 m, 702 vs, 664 m, 565 m, 457 s, 434 m, 417 w.

Preparations of Tb(BTC)$(H_2O)\cdot(DMF)_{1.1}$ (2a and 2b). Both small- and large-scale crystals of **2a** and **2b** were synthesized by the procedures similar to those of **1a** and **1b**, except that $Y(NO_3)_3\cdot 6H_2O$ was replaced by $Tb(NO_3)_3\cdot 6H_2O$ with the same molar amount. The yield of small-scale synthesis: ∼49%. Calcd for $Tb(C_9H_3O_6)(H_2O)(C_3H_6ON)_{1.1}$: C, 31.88; H, 2.53; N, 3.33. Found: C, 32.05; H, 2.51; N, 3.46. IR (cm^{-1}): 1613 m, 1572 w, 1536 w, 1433 m, 1366 s, 1100 w, 939 w, 768 s, 716 m, 702 vs, 662 w, 556 m, 459 s, 426 s.

Preparations of Dy(BTC)$(H_2O)\cdot(DMF)_{1.1}$ (3a and 3b). Both small- and large-scale crystals of **3a** and **3b** were synthesized by the procedures similar to those of **1a** and **1b**, except that $Y(NO_3)_3\cdot 6H_2O$ was replaced by $Dy(NO_3)_3\cdot 6H_2O$ with the same molar amount. The yield of small-scale synthesis: ∼53%. Calcd for $Dy(C_9H_3O_6)(H_2O)(C_3H_6ON)_{1.1}$: C, 31.64; H, 2.51; N, 3.30. Found: C, 31.22; H, 2.59; N, 3.34. IR (cm^{-1}): 1611 m, 1572 w, 1534 w, 1435 m, 1373 s, 1100 w, 939 w, 770 s, 714 m, 702 vs, 666 m, 559 s, 455 s, 428 m, 417 w.

Preparations of Er(BTC)$(H_2O)\cdot(DMF)_{1.1}$ (4a and 4b). Both small- and large-scale crystals of **4a** and **4b** were synthesized by the procedures similar to those of **1a** and **1b**, except that $Y(NO_3)_3\cdot 6H_2O$ was replaced by $Er(NO_3)_3\cdot 6H_2O$ with the same molar amount. The yield of small-scale synthesis: ∼46%. Calcd for $Er(C_9H_3O_6)(H_2O)(C_3H_6ON)_{1.1}$: C, 31.32; H, 2.48; N, 3.27. Found: C, 31.28; H, 2.54; N, 3.33. IR (cm^{-1}): 1611 m, 1572 w, 1536 w, 1433 m, 1372 s, 1103 w, 939 w, 770 s, 714 m, 702 vs, 666 m, 563 s, 455 s, 434 m, 417 w.

Preparations of Yb(BTC)$(H_2O)\cdot(DMF)_{1.1}$ (5a and 5b). Both small and large-scale crystals of **5a** and **5b** were synthesized by the procedures similar to those of **1a** and **1b**, except that $Y(NO_3)_3\cdot 6H_2O$ was replaced by $Yb(NO_3)_3\cdot 6H_2O$ with the same molar amount. The yield of small-scale synthesis: ∼42%. Calcd for $Yb(C_9H_3O_6)(H_2O)(C_3H_6ON)_{1.1}$: C, 30.94; H, 2.45; N, 3.23. Found: C, 31.47; H, 2.39; N, 3.39. IR (cm^{-1}): 1615 m, 1576 w, 1539 w, 1437 m, 1373 s, 1098 w, 939 w, 772 s, 714 m, 702 vs, 667 m, 565 s, 459 s, 434 m, 419 w.

X-ray Crystallography. Single-crystal X-ray diffraction data for compounds **1**−**5** were collected on a R-AXIS RAPID II diffractometer at room temperature with Mo Kα radiation (λ = 0.71073 Å).[9] All the structures were solved by direct methods using the SHELXS program of the SHELXTL package and refined by full-matrix least-squares methods with SHELXL.[10] Metal atoms in each compound were located from the *E*-maps, and other non-hydrogen atoms were located in successive difference Fourier syntheses, where they were refined with anisotropic thermal parameters on F^2. Hydrogen atoms were located at geometrically calculated positions and refined with isotropic thermal parameters. Isolated solvents within the channels were not crystallographically well-defined. The uncoordinated DMF molecules were determined on the basis of TGA and elemental microanalysis, and the data were treated with the SQUEEZE routine within PLATON.[11] Crystallographic data and structural refinements for compounds **1**−**5** are summarized

(5) (a) Zhang, J.; Chen, S.; Wu, T.; Feng, P.; Bu, X. *J. Am. Chem. Soc.* **2008**, *130*, 12882. (b) Jiang, H. L.; Liu, B.; Xu, Q. *Cryst. Growth Des.* **2010**, *10*, 806.

(6) (a) Davis, M. E. *Nature* **2002**, *417*, 813. (b) Maspoch, D.; Ruiz-Molina, D.; Veciana, J. *Chem. Soc. Rev.* **2007**, *36*, 770.

(7) (a) Ayyappan, S.; Bu, X.; Cheetham, A. K.; Rao, C. N. R. *Chem. Mater.* **1998**, *10*, 3308. (b) Hao, X. R.; Wang, X.-L.; Qin, C.; Su, Z. M.; Wang, E. B.; Lan, Y. Q.; Shao, K. Z. *Chem. Commun.* **2007**, 4620. (c) Zhang, J.; Wu, T.; Chen, S.; Feng, P.; Bu, X. *Angew. Chem., Int. Ed.* **2009**, *48*, 3486. (d) Zhang, W.; Ye, H.-Y.; Xiong, R.-G. *Coord. Chem. Rev.* **2009**, *253*, 2980.

(8) (a) Guo, X.; Zhu, G.; Li, Z.; Sun, F.; Yang, Z.; Qiu, S. *Chem. Commun.* **2006**, 3172. (b) Rosi, N. L.; Kim, J.; Eddaoudi, M.; Chen, B.; O'Keeffe, M.; Yaghi, O. M. *J. Am. Chem. Soc.* **2005**, *127*, 1504. (c) Luo, J.; Xu, H.; Liu, Y.; Zhao, Y.; Daemen, L. L.; Brown, C.; Timofeeva, T. V.; Ma, S.; Zhou, H.-C. *J. Am. Chem. Soc.* **2008**, *130*, 9626. (d) Gustafsson, M.; Bartoszewicz, A.; Martín-Matute, B.; Sun, J.; Grins, J.; Zhao, T.; Li, Z.; Zhu, G.; Zou, X. *Chem. Mater.* **2010**, *22*, 3316.

(9) Higashi, T. *Program for Absorption Correction*; Rigaku Corporation: Tokyo, Japan, 1995.

(10) Sheldrick, G. M. *SHELXTL NT, Program for Solution and Refinement of Crystal Structures*, version 5.1; University of Göttingen: Göttingen, Germany, 1997.

(11) Spek, A. L. *J. Appl. Crystallogr.* **2003**, *36*, 7.

Table 1. Crystallographic Parameters for Compounds **1**−**5** from Single-Crystal X-ray Diffraction

	1b	**2b**	**3b**	**4a**	**4b**	**5b**
formula	$C_9H_5O_7Y$	$C_9H_5O_7Tb$	$C_9H_5DyO_7$	$C_9H_5ErO_7$	$C_9H_5ErO_7$	$C_9H_5O_7Yb$
fw	314.04	384.05	387.63	392.39	392.39	398.17
crystal system	tetragonal	tetragonal	tetragonal	tetragonal	tetragonal	tetragonal
space group	$P4_322$	$P4_322$	$P4_322$	$P4_122$	$P4_322$	$P4_322$
a (Å)	10.2900(15)	10.3300(15)	10.3200(15)	10.2700(15)	10.2670(15)	10.2400(14)
c (Å)	14.500(3)	14.510(3)	14.500(3)	14.460(3)	14.462(3)	14.420(3)
V (Å^3)	1535.3(4)	1548.3(4)	1544.3(4)	1525.1(4)	1524.5(4)	1512.0(4)
Z	4	4	4	4	4	4
d_{calcd} (g/cm^3)	1.354	1.639	1.659	1.700	1.701	1.740
μ (mm^{-1})	3.812	4.581	4.852	5.516	5.519	6.199
F(000)	612	712	716	724	724	732
Flack parameter	0.00(2)	−0.01(2)	0.04(3)	0.00(3)	0.036(18)	0.001(17)
reflns collected	14801	15015	15151	14910	14777	14561
independent reflns	1755 [R_{int} = 0.0957]	1768 [R_{int} = 0.0468]	1767 [R_{int} = 0.0490]	1740 [R_{int} = 0.0387]	1734 [R_{int} = 0.0458]	1716 [R(int) = 0.0447]
obsd data [I > 2σ(I)]	1475	1682	1647	1623	1699	1672
completeness to θ	99.3%	99.1%	99.3%	99.3%	98.7%	98.7%
data/restraints/parameters	1755/0/83	1768/0/80	1767/0/80	1740/0/80	1734/0/80	1716/0/80
GOF on F^2	1.129	1.096	1.133	1.213	1.099	1.097
R1, wR2 [I > 2σ(I)]	0.0546, 0.1397	0.0188, 0.0453	0.0254, 0.0670	0.0215, 0.0585	0.0167, 0.0403	0.0165, 0.0408
R1, wR2 (all data)	0.0734, 0.1594	0.0210, 0.0458	0.0287, 0.0681	0.0249, 0.0593	0.0173, 0.0404	0.0171, 0.0410

Table 2. Selected Bond Lengths (Å) for Compounds **1**−**5**[a]

	4a
Ln(1)−O(2)#1	2.276(4)
Ln(1)−O(2)#2	2.276(4)
Ln(1)−O(3)#3	2.282(4)
Ln(1)−O(3)#4	2.282(4)
Ln(1)−O(1)#5	2.294(4)
Ln(1)−O(1)	2.294(4)
Ln(1)−O(4)	2.376(6)

	1b	**2b**	**3b**	**4b**	**5b**
Ln(1)−O(1)#1	2.279(5)	2.319(3)	2.308(4)	2.272(3)	2.252(3)
Ln(1)−O(1)#2	2.279(5)	2.319(3)	2.308(4)	2.272(3)	2.252(3)
Ln(1)−O(2)#3	2.291(5)	2.320(3)	2.313(4)	2.281(2)	2.255(3)
Ln(1)−O(2)#4	2.291(5)	2.320(3)	2.313(4)	2.281(2)	2.255(3)
Ln(1)−O(3)#5	2.298(5)	2.318(3)	2.313(4)	2.286(3)	2.270(3)
Ln(1)−O(3)	2.298(5)	2.318(3)	2.313(4)	2.286(3)	2.270(3)
Ln(1)−O(4)	2.375(9)	2.428(5)	2.403(7)	2.386(4)	2.357(4)

[a] Symmetry codes for **4a**: #1 $x, y+1, z$; #2 $-y, -x+1, -z+1/4$; #3 $y+1, -x+1, z-1/4$; #4 $x, -y, -z+1/2$; #5 $-y+1, -x+1, -z+1/4$. Symmetry codes for **1b**, **2b**, **3b**, **4b**, and **5b**: #1 $y-1, x, -z+1/4$; #2 $x, y-1, z$; #3 $-y+1, x, z-1/4$; #4 $x, -y+1, -z+1/2$; #5 $y, x, -z+1/4$.

in Table 1. Important bond lengths are listed in Table 2. More details on the crystallographic studies as well as atom displacement parameters are given in the Supporting Information.

Results and Discussion

Structural Descriptions. Treatments of lanthanide(III) nitrates and 1,3,5-benzenetricarboxylate (BTC) in mixed solvents of DMF and aqua inside a Teflon-lined autoclave at 105 °C for 24 h yielded needlelike chiral lanthanide crystals of $Ln(BTC)(H_2O)\cdot DMF_{1.1}$ (Ln = Y, Tb, Dy, Er, Yb). Fortunately, the enantiopure counterparts of each compound can be separated manually. Single-crystal X-ray diffraction analyses[9,10] reveal that the structures of compounds Ln-**a** and Ln-**b** are enantiomers. Their unit-cell dimensions, volumes, related bond distances, and angles are only slightly different. These compounds are isostructural, and therefore, erbium compound of **4b** will be discussed in detail as a representative. As shown in Figure 1a, there is one crystallographically unique erbium(III) ion, an independent BTC ligand and one water molecule in the asymmetric unit. The erbium(III) ion is coordinated by seven oxygen atoms with six oxygen atoms from six carboxylate groups of six BTC ligands and one oxygen atom from the terminal water molecule in a distorted pentagonal-bipyramidal coordination sphere, in which the four O atoms from four BTC anions (O1F, O1I, O3C, and O3G) and one O atom from the water molecule (O4C) to make up the basal plane, while the axial positions are occupied by two O atoms (O2A and O2H) from another two BTC molecules (Figure 1b). The carboxylic O−Er bond distances are in the range of 2.272(3)−2.286(3) Å, slightly shorter than that of water O−Er (2.386(4) Å), all of which are comparable to reported erbium MOFs.[12] The O−Er(III)−O bond angles range from 69.21(8) to 165.06(16)°. The BTC ligand bridges to six Er(III) ions and each carboxylic oxygen connects one Er(III) (Figure 1a). Such connection fashion of Er(III) ion and BTC ligand leads to interesting 1D helical strands in the structure. As shown in Figure 2a, the carboxylic oxygen atoms of BTC ligands bridge adjacent Er(III) ions to form three-stranded helical chains running along the crystallographic 4_3 axis with a very long helical pitch of 43.39 Å. The left and right helical inorganic chains along the c direction appear in the enantiomers, respectively (Figure 2a). The occurrence of helical strands is attributable to the steric orientation of the carboxylate groups of BTC ligand. These helical chains are further linked with each other through BTC ligands to form a 3D framework with 1D helical channels of between 6×6 Å^2 and 7×7 Å^2 along the c axis, in which terminal water and free DMF molecules are located (Figure 2b). The effective free volumes are 44.5%, 44.8%, 47.7%, 44.2%, and 45.7% in compounds **1**, **2**, **3**, **4** and **5**, respectively, calculated by PLATON.[11]

Topological Analysis. A better insight into the nature of the involved framework can be achieved by the application of a topological approach. As described above, each Ln(III) ion is linked by six BTC ligands and each BTC

(12) (a) Zhang, Z.-H.; Song, Y.; Okamura, T.; Hasegawa, Y.; Sun, W.-Y.; Ueyama, N. *Inorg. Chem.* **2006**, *45*, 2896. (b) Cheng, J.-W.; Zheng, S.-T.; Yang, G.-Y. *Dalton Trans.* **2007**, 4059.

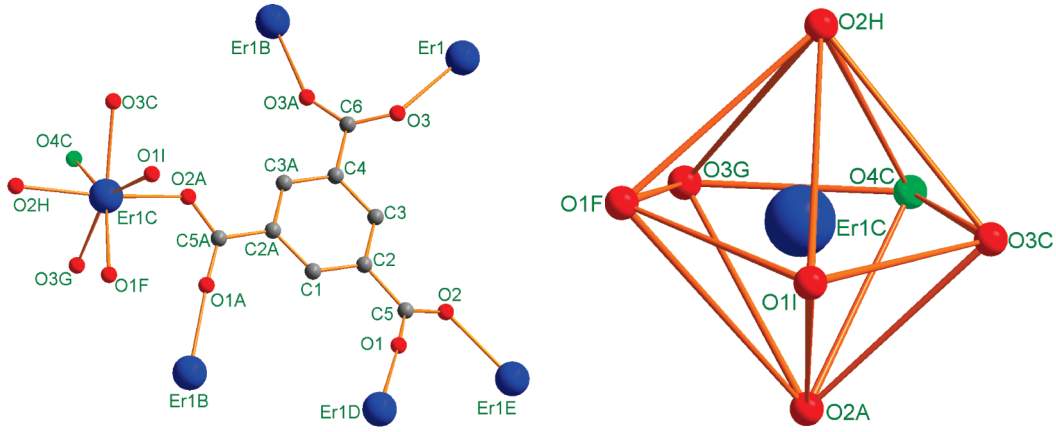

Figure 1. (a) Coordination environment of erbium center and the binding fashion of BTC ligand and (b) the distorted pentagonal-bipyramidal coordination sphere of the Er(III) ion. Symmetry codes: A $-x, y, -z$; B $-y, x, z-1/4$; C $-x, -y+1, z-1/2$; D $x, y+1, z$; E $y, -x+1, z+1/4$; F $-x, -y+2, z-1/2$; G $-y, -x+1, -z-1/4$; H $y-1, -x+1, z-3/4$; I $-y+1, -x+1, -z-1/4$.

ligand bridges six Ln(III) ions. Therefore, both Ln(III) and BTC ligand can be regarded as six-connected nodes, and the whole network can be extended to an unusual 3D (6,6)-connected net with the Schläfli symbol of $(4^{13}\cdot6^2)$-$(4^8\cdot6^7)$,[13] as displayed in Figure 3. So far, many uninodal network topologies, such as three-, four-, and six-connected topologies have been reported,[14] and some MOFs with mixed-low connected topologies have been reported, for example, Pt_3O_4, boracite, PtS, rutile, pyrite, anatase, and so on.[15] However, MOFs with binodal high-connected structures are extremely rare, for example, (3,8)- and (3,9)-connected frameworks.[16] The (6,6)-connected framework, compared to the above-mentioned nets, is more difficult to achieve because it contains two kinds of high-connected nodes. As far as we know, this topology has not been observed in metal−organic frameworks yet

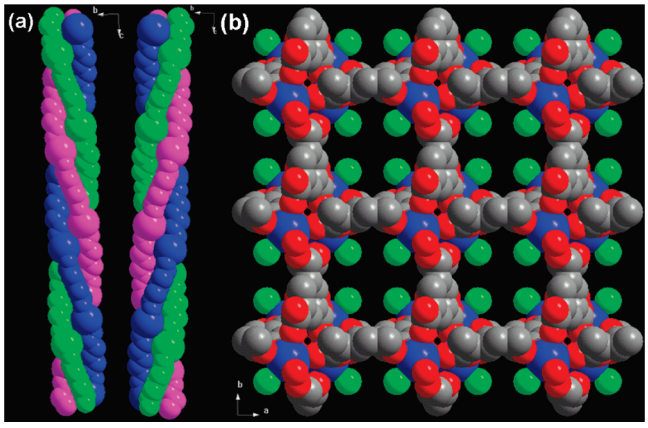

Figure 2. (a) Left-handed (in structures with $P4_122$ space group) and right-handed (in structures with $P4_322$ space group) helical chains along the *c*-axis in enantiomers. (b) View of the 3D structure with $P4_322$ space group along the *c*-axis, exhibiting 1D helical channels of about 6−7 Å for each side, and accessible Ln^{3+} sites can be obtained after removing the coordinated aqua molecules, which denoted as green. The H atoms and free DMF molecules are omitted for clarity; Ln, O, and C atoms are drawn as blue, red, and gray circles, respectively.

to date, and it is quite distinct from the limited (6,6)-connected topology previously reported with α-polonium or NiAs-type structures.[17]

Thermogravimetric Analysis (TGA). TGA experiments were conducted to determine the thermal stability of all the compounds, which is an important aspect for metal−organic frameworks.[18] TG analyses indicate that all these compounds have very high thermal stability (Figure 4). The compounds release their terminal water and free DMF molecules ranging from room temperature to 315−345 °C in air, to give guest-free frameworks of Ln(BTC). After that, a long plateau appears and all the compounds are thermally stable up to over 450 °C, followed by the degradation of the framework. The powder XRD patterns of the guest free phases, showing very good crystallinity,

(13) (a) Wells, A. F. *Three-Dimensional Nets and Polyhedra*; Wiley: New York, 1977. (b) Batten, S. R.; Robson, R. *Angew. Chem., Int. Ed.* **1998**, *37*, 1460. (c) Ockwig, N. W.; Delgado-Friedrichs, O.; O'Keeffe, M.; Yaghi, O. M. *Acc. Chem. Res.* **2005**, *38*, 176.

(14) (a) Blake, A. J.; Champness, N. R.; Hubberstey, P.; Li, W. S.; Withersby, M. A.; Schröder, M. *Coord. Chem. Rev.* **1999**, *183*, 117. (b) Batten, S. R.; Hoskins, B. F.; Robson, R. *Chem.—Eur. J.* **2000**, *6*, 156. (c) Carlucci, L.; Cozzi, N.; Ciani, G.; Moret, M.; Proserpio, D. M.; Rizzato, S. *Chem. Commun.* **2002**, 1354. (d) Moulton, B.; Lu, J. J.; Zaworotko, M. J. *J. Am. Chem. Soc.* **2001**, *123*, 9224. (e) Feng, R.; Jiang, F.-L.; Chen, L.; Yan, C.-F.; Wu, M.-Y.; Hong, M.-C. *Chem. Commun.* **2009**, 5296.

(15) (a) Batten, S. R.; Hoskins, B. F.; Robson, R. *Chem. Commun.* **1991**, 445. (b) Abrahams, B. F.; Batten, S. R.; Hamit, H.; Hoskins, B. F.; Robson, R. *Angew. Chem., Int. Ed.* **1996**, *35*, 1690. (c) Chui, S. S. Y.; Lo, S. M. F.; Charmant, J. P. H.; Orpen, A. G.; Williams, I. D. *Science* **1999**, *283*, 1148. (d) Xiang, S. C.; Wu, X. T.; Zhang, J. J.; Fu, R. B.; Hu, S. M.; Zhang, X. D. *J. Am. Chem. Soc.* **2005**, *127*, 16352.

(16) (a) Chun, H.; Kim, D.; Dybtsev, D. N.; Kim, K. *Angew. Chem., Int. Ed.* **2004**, *43*, 971. (b) Zhang, X. M.; Fang, R. Q.; Wu, H. S. *J. Am. Chem. Soc.* **2005**, *127*, 7670. (c) Hill, R. J.; Long, D. L.; Champness, N. R.; Hubberstey, P.; Schröder, M. *Acc. Chem. Res.* **2005**, *38*, 335. (d) Natarajan, S.; Mahata, P. *Chem. Soc. Rev.* **2009**, *38*, 2304.

(17) (a) Hoskins, B. F.; Robson, R.; Slizys, D. A. *Angew. Chem., Int. Ed.* **1997**, *36*, 2752. (b) Chae, H.-K.; Eddaoudi, M.; Kim, J.-K.; Hauck, S. I.; Hartwig, J. F.; O'Keeffe, M.; Yaghi, O. M. *J. Am. Chem. Soc.* **2001**, *123*, 11482. (c) Wang, Z.; Zhang, X.; Batten, S. R.; Kurmoo, M.; Gao, S. *Inorg. Chem.* **2007**, *46*, 8439. (d) Bai, Y.-L.; Tao, J.; Huang, R.-B.; Zheng, L.-S.; Zheng, S.-L.; Oshida, K.; Einaga, Y. *Chem. Commun.* **2008**, 1753. (e) Cañdillas-Delgado, L.; Marín, T.; Fabelo, O.; Pasán, J.; Delgado, F. S.; Lloret, F.; Julve, M.; Ruiz-Pérez, C. *Chem.—Eur. J.* **2010**, *16*, 4037.

(18) (a) De Lill, D. T.; Cahill, C. L. *Chem. Commun.* **2006**, 4946. (b) Zou, R. Q.; Zhong, R. Q.; Du, M.; Kiyobayashi, T.; Xu, Q. *Chem. Commun.* **2007**, 2467.

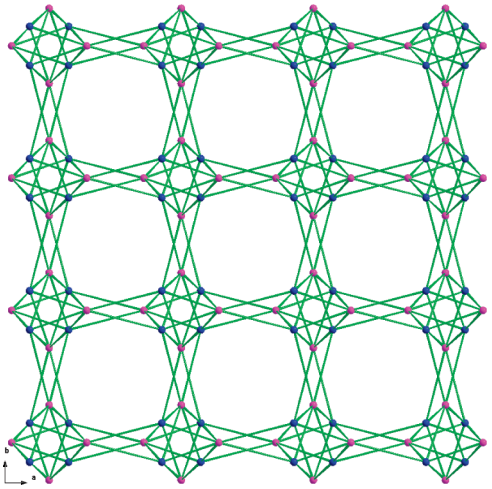

Figure 3. Topological view of the 3D structure with $P4_322$ space group.

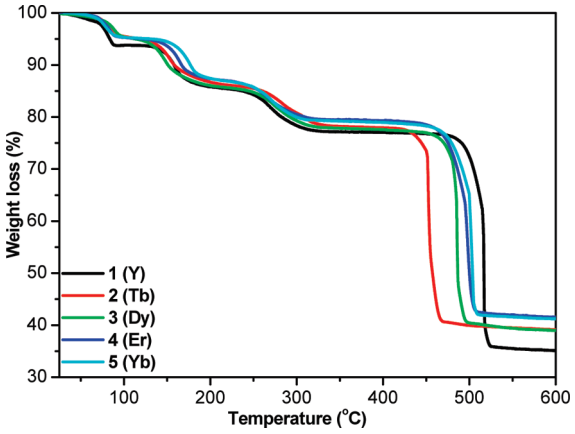

Figure 4. TG curves for compounds **1**−**5**.

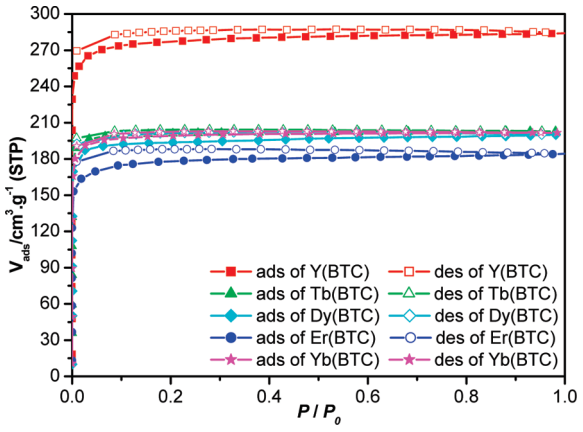

Figure 5. N_2 sorption isotherms for compounds **1**−**5** at 77 K; ads = adsorption and des = desorption.

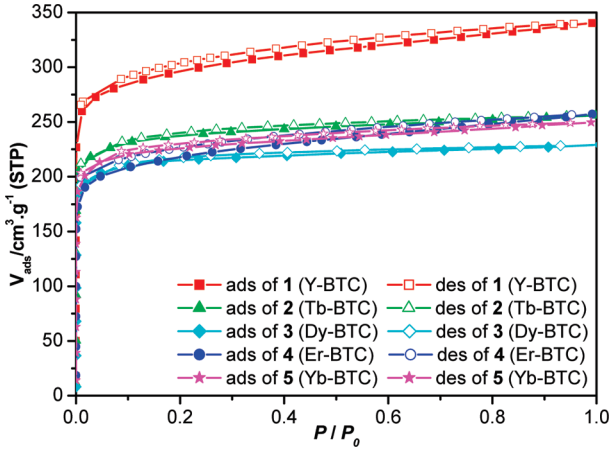

Figure 6. Ar sorption isotherms for compounds **1**−**5** at 87 K; ads = adsorption and des = desorption.

are almost identical to those of as-synthesized samples, which indicate that their frameworks can be retained and accessible metal sites can be obtained by removal of free DMF and terminal water molecules after thermal activation. Generally, degradation of the organic components of MOFs typically starts at moderate temperatures (200−350 °C),[19] leading to the decomposition of these organic ligands-related MOFs. Only limited MOFs were reported to be stable above 350 °C and the reasons for this still remain unclear,[18−21] although it is usually accepted that the Si- and Zr- based MOFs have higher thermal stability.[20b,21a] It was also considered that the compact networks of the host frameworks could play a crucial role in determining their thermal stabilities. So far, all rarely reported carboxylic-based MOFs with thermal stability higher than 450 °C almost have few accessible void spaces.[18,21] To the best of our knowledge, the present series of compounds are the first carboxylic-based MOFs with both high porosity and high thermal stability of over 450 °C in air, which may highly facilitate their functional applications.[20c] It is assumed that the strong metal-carboxylate interactions tighten the backbone of the ligand to enhance the resistance to pyrolysis.

Adsorption Properties. To examine the pore characteristics and gas storage capability, the sorption properties of the desolvated **1**−**5** have been examined with N_2, Ar, and H_2 gases. The N_2 sorption measurements of desolvated **1**−**5** at 77 K exhibit a type-I isotherm (Figure 5), which indicates the typical characteristic of microporous material. The BET surface areas are fitted to be 1080, 786, 757, 676, and 774 m^2/g, respectively, for thermal activated Y, Tb, Dy, Er, and Yb compounds with corresponding pore volumes of 0.44 (**1**), 0.31 (**2**), 0.31 (**3**), 0.28 (**4**), and 0.31 cm^3/g (**5**), which are significantly higher than those of reported Dy and Tb compounds.[8a,b] On the contrary, although others reported Y-BTC compound adsorbed very few nitrogen gas molecules at 77 K,[8c] our results showed Y-BTC has the highest surface area among these MOFs. The argon sorption isotherms were collected at 87 K (Figure 6). The adsorption−desorption

(19) (a) Xue, D.-X.; Lin, J.-B.; Zhang, J.-P.; Chen, X.-M. *CrystEngComm* **2009**, *11*, 183. (b) Gao, Q.; Jiang, F.-L.; Wu, M.-Y.; Huang, Y.-G.; Wei, W.; Hong, M.-C. *Cryst. Growth Des.* **2010**, *10*, 184.

(20) (a) Perles, J.; Iglesias, M.; Martin-Luengo, M.-A.; Monge, M. A.; Ruiz-Valero, C.; Snejko, N. *Chem. Mater.* **2005**, *17*, 5837. (b) Cavka, J. H.; Jakobsen, S.; Olsbye, U.; Guillou, N.; Lamberti, C.; Bordiga, S.; Lillerud, K. P. *J. Am. Chem. Soc.* **2008**, *130*, 13850. (c) Ma, S.; Wang, X.-S.; Yuan, D.; Zhou, H.-C. *Angew. Chem., Int. Ed.* **2008**, *47*, 4130.

(21) (a) Yang, S. Y.; Long, L. S.; Jiang, Y. B.; Huang, R. B.; Zheng, L. S. *Chem. Mater.* **2002**, *14*, 3229. (b) Sun, D.; Ma, S.; Ke, Y.; Petersen, T. M.; Zhou, H.-C. *Chem. Commun.* **2005**, 2663. (c) Banerjee, D.; Borkowski, L. A.; Kim, S. J.; Parise, J. B. *Cryst. Growth Des.* **2009**, *9*, 4922.

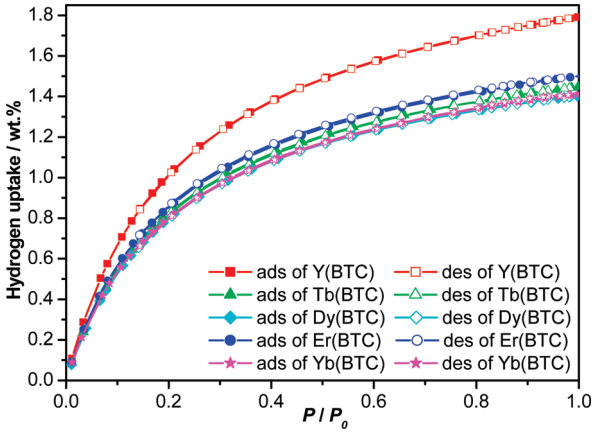

Figure 7. Total gravimetric hydrogen sorption isotherms for compounds **1**−**5** at 77 K; ads = adsorption and des = desorption.

isotherms of all compounds also showed a typical Type-I behavior, and the values are naturally higher than those of N_2 adsorption. The considerable surface areas, high free volumes, nanosized free windows, accessible exposed metal sites and very high thermal stability for these MOFs could endow them very high potentials in gas storage, catalysis, and other functional applications for the pores.[1d,4,22]

The high porosities and surface areas in these MOFs prompted us to evaluate their hydrogen adsorption performances. Low-pressure hydrogen sorption isotherms of the activated samples at 77 K revealed reversible hydrogen adsorption as shown Figure 7. At 77 K and 1 atm, the excess gravimetric hydrogen uptake capacity of compounds **1**−**5** reaches to 1.79, 1.45, 1.40, 1.51, and 1.41 wt % for Y, Tb, Dy, Er and Yb, respectively, compounds. These values are considerably high compared to those of reported MOFs thus far under the same conditions,[23] and are consistent with the estimated large pore volumes. The values for compounds Y (**1**) and Dy (**3**) are also slightly higher than those of the previously reported data.[8a,c]

Conclusion

In summary, we have systematically synthesized and structurally characterized a series of isostructural lanthanide-organic framework enantiomers, $Ln(BTC)(H_2O)\cdot(DMF)_{1.1}$ (Ln = Y **1a**, **1b**; Tb **2a**, **2b**; Dy **3a**, **3b**; Er **4a**, **4b**; Yb **5a**, **5b**, BTC = 1,3,5-benzenetricarboxylate), and investigated their thermal stabilities and gas sorption properties. All these MOFs exhibit exceptional thermal stability of over 450 °C in air. Moreover, all compounds are highly porous with a surface area of 1080 (**1**), 786 (**2**), 757 (**3**), 676 (**4**), and 774 m^2/g (**5**), respectively (N_2 data). A hydrogen uptake of 1.79 (**1**), 1.45 (**2**), 1.40 (**3**), 1.51 (**4**), and 1.41 wt % (**5**) is achieved at 77 K (1 atm), showing the superior H_2 sorption capability among the group of MOFs. The easily scalable preparation, highly porous characteristic, nanosized pore/channel openings, accessible exposed metal sites as well as very high thermal stability of these MOF enantiomers endow them very high potential for broad applications in gas storage, catalysis, etc.

Acknowledgment. The authors thank the reviewers for their valuable suggestions and AIST and JSPS for financial support. H.-L.J. thanks JSPS for a postdoctoral fellowship.

Supporting Information Available: X-ray crystallographic files for compounds **1**−**5** in CIF format and figures showing powder X-ray diffraction patterns and H_2 adsorption and desorption curves. This material is available free of charge via the Internet at http://pubs.acs.org.

(22) Murray, L. J.; Dincă, M.; Long, J. R. *Chem. Soc. Rev.* **2009**, *38*, 1294.

(23) (a) Lee, J. Y.; Pan, L.; Kelly, S. P.; Jagiello, J.; Emge, T. J.; Li, J. *Adv. Mater.* **2005**, *17*, 2703. (b) Chun, H.; Dybtsev, D. N.; Kim, H.; Kim, K. *Chem.—Eur. J.* **2005**, *11*, 3521. (c) Ma, S. Q.; Zhou, H.-C. *Chem. Commun.* **2010**, *46*, 44.